Research Article | Vol. 27, No. 24 / 25 November 2019 / Optics Express 34769
Optics EXPRESS

# On the effect of third-order dispersion on phase-matched terahertz generation via interfering chirped pulses

SPENCER W. JOLLY,[1,2,6,*] FREDERIKE AHR,[3,4] KOUSTUBAN RAVI,[3,5] NICHOLAS H. MATLIS,[3] FRANZ X. KÄRTNER,[3,4,5] AND ANDREAS R. MAIER[1]

[1]*Center for Free-Electron Laser Science & Department of Physics, Universität Hamburg, Luruper Chaussee 149, 22761 Hamburg, Germany*
[2]*Institute of Physics of the ASCR, ELI-Beamlines project, Na Slovance 2, 18221 Prague, Czech Republic*
[3]*Deutsches Elektronen Synchrotron (DESY) & Center for Free-Electron Laser Science, Notkestraße 85, 22607 Hamburg, Germany*
[4]*Department of Physics, Universität Hamburg, Luruper Chaussee 149, 22761 Hamburg, Germany*
[5]*Research Laboratory of Electronics, Massachusetts Institute of Technology, 77 Massachusetts Avenue, Cambridge, MA 02139, USA*
[6]*Currently LIDYL, CEA, CNRS, Université Paris-Saclay, CEA Saclay, 91 191 Gif-sur-Yvette, France*
[*]*spencer.jolly@cea.fr*

**Abstract:** High-energy narrowband terahertz (THz) pulses, relevant for a plethora of applications, can be created from the interference of two chirped-pulse drive lasers. The presence of third order dispersion, an intrinsic feature of many high-energy drive lasers, however, can significantly reduce the optical-to-THz conversion efficiency and have other undesired effects. Here, we present a detailed description of the effect of third-order dispersion (TOD) in the pump pulse on the generation of THz radiation via phase-matching of broadband highly chirped pulse trains. Although the analysis is general, we focus specifically on parameters typical to a Ti:Sapphire chirped-pulse amplification laser system for quasi-phase-matching in periodically-poled lithium niobate (PPLN) in the range of THz frequencies around 0.5 THz. Our analysis provides the tools to optimize the THz generation process for applications requiring high energy and to control it to produce desired THz waveforms in a variety of scenarios.



## 1. Introduction

The last two decades have seen a tremendous surge in development of terahertz (THz) sources of high-energy and high-peak-field for applications ranging from linear and nonlinear spectroscopy [1], to compact electron acceleration [2–7] and manipulation [8–12]. Broadband or single-cycle pulses produce the highest peak-field, but for specific electron acceleration applications, multi-cycle, narrowband pulses are of particular interest [2,3]. Sources based on optically driven difference frequency generation (DFG) are very promising for these applications, especially due to relatively high optical-to-terahertz conversion efficiencies.

Achieving high conversion efficiency requires high incident fluence and proper phase-matching of the nonlinear process. Quasi-phase-matching (QPM) in periodically poled lithium niobate (PPLN) [13–15] is a promising candidate for narrowband THz generation, due to the high nonlinearity in lithium niobate, the transparency for optical light around 800 nm, and the availability of very high energy driving pulses in that wavelength range. The chirp-and-delay technique—whereby two copies of a chirped laser pulse are combined with a time delay in a photoconducting element or nonlinear crystal—is a succesful approach to provide the necessary pulse format for DFG while avoiding parasitic nonlinear processes and staying below the damage

#377350 https://doi.org/10.1364/OE.27.034769
Journal © 2019 Received 6 Sep 2019; revised 13 Oct 2019; accepted 14 Oct 2019; published 12 Nov 2019

Optics EXPRESS

threshold while pumping with higher fluence pulses than when pumping with compressed pulses [16,17]. Recent experiments from our team using PPLN showed that the method of chirp-and-delay using pulse copies from a broadband Ti:Sapphire-based system can generate THz in the 0.3–0.8 THz frequency range with energies up to 40 $\mu$J [18].

However, there were known complexities in the results in Ahr et al. [18] which implied that details of the complete process were not yet fully understood. First and foremost, the efficiency of the process measured to be in the 0.1 % range was not as high as in ideal theoretical predictions [15], showing efficiencies up to the 1 % range. The THz output as a function of delay was peaked as expected based on the chirp rate and the poling period of the crystal in use, but also showed complex features that were not at the time explained. Additionally, there were nuances that led us to believe that the full pump pulse was not taking part in the process; specifically that the modification of the pump spectrum, which can act as a fingerprint of the nature of the nonlinear process, did not occur in the entire pump spectrum, but only the central portion.

The exact effect of the higher-order phase will be derived analytically, but the concept can already be visualized using the Wigner-style plots common in the field of DFG. Figure 1 shows two broadband chirped pulses which are separated by a delay $\Delta t$, providing the necessary difference frequency content for DFG. This simple plot shows the general effect of TOD on the process. In the ideal case of Fig. 1(a), the purely linear-chirped pulse copies produce a localized difference frequency $\Delta\omega$ where the majority of the nonlinear polarization is matched to the nonlinear medium at $\Omega$ and within the bandwidth of the nonlinear process $\delta\Omega$ (seen in Fig. 1(b)). When TOD is included in the picture as in Fig. 1(c), the pulses are no longer purely linear, and now less of the energy of the pump pulses is within the quasi-phase-matching bandwidth (Fig. 1(d)).

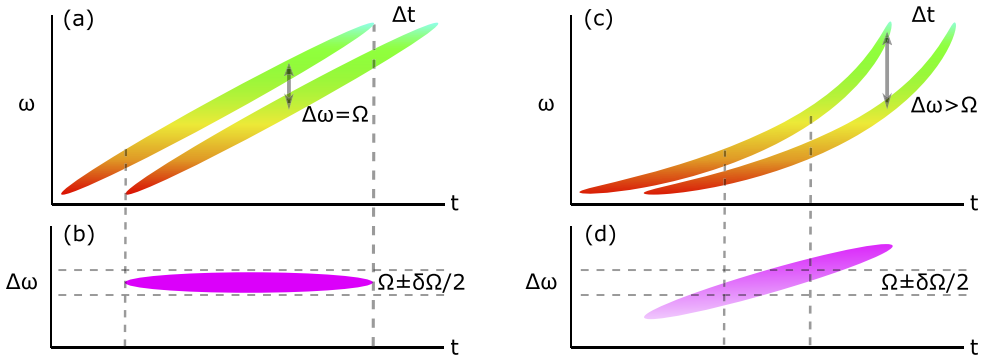


**Fig. 1.** Chirp and delay concept including now the general effect of higher order phase. (a) and (b) are the separate overlapped pump pulses without any TOD and the resulting difference frequency $\Delta\omega$, respectively. $\Omega$ corresponds to the phase-matched THz angular frequency, and $\Delta\omega$ is the bandwidth of the phase-matching process. (c) and (d) are the same now with TOD (not to scale) showing that less of the overall difference frequency content is within the THz bandwidth $\delta\Omega$. The horizontal dashed lines represent the bandwidth of the phase-matching process, and the vertical dashed lines represent the region in time that is within that bandwidth.

This manuscript outlines how principally the higher order spectral phase on the near-infrared (NIR) pump—but also the complex train of pulses from the specific experimental setup used in Ahr et al. [18]—contribute to these nuances and the decreased efficiency compared to the ideal prediction. This specific effect was compensated for in recent work by our group [19], where we produced 600 $\mu$J of total narrowband THz energy. This current work provides the detailed explanation of the initial limitations and complexities observed in Ahr et al. [18] while also

Optics EXPRESS

providing more detail and outlook than in the milestone result in Jolly et al. [19]. The effect of the TOD on difference frequency generation with direct phase-matching will also be discussed, along with implications on the temporal properties of generated THz.

We start in Section 2 with a discussion of the theory of phase-matching and how material and drive laser properties have a direct impact on the DFG output. We then tackle in more detail the specific impact of TOD and pulse-train structure on the total drive laser field in Section 3. In Section 4 we discuss the signature of the TOD and pulse-train structure in experimental data. Using the derivation and experimental confirmation of these effects we then discuss the implications on THz generation efficiency (Section 5), THz pulse envelope (Section 6), and THz pulse phase (Section 7), with a final section containing concluding remarks (Section 8).

As a technical note, the produced total intensity profile of overlapped chirped pulses has modulations that have a frequency corresponding to the instantaneous difference frequency, which are sometimes referred to as a pulse-train. This manuscript refers to the train of overlapped macroscopic pulses (whether two or more) as a pulse-train, and rather refers to the microscopic train of pulses (sub-pulses) created from the pulse beating as modulations on the intensity envelope. This will be clarified in Section 3.

## 2. Properties of phase matching with chirped-and-delayed pulses

An expression for the THz field amplitude $A_{\mathrm{THz}}$ generated from chirped and delayed pulses was provided in [15]. The derivation uses the wave equation in the spectral domain including THz absorption in the nonlinear medium. An effective second order nonlinearity $\chi_2^{\mathrm{eff}} = 2\chi_2/\pi$ is assumed, where $\chi_2$ is the bulk nonlinearity, which is necessary in the case of quasi-phase matching [20]. Ignoring group velocity dispersion and the effect of the THz generation on the spectrum of the optical pump, the generated THz field amplitude along the propagation direction $z$ is

$$A_{\mathrm{THz}}(\Omega,\ z) = \mathcal{F}_{t\to\omega}\left[|A_{\mathrm{opt}}(t)|^2\right]\frac{i\Omega\chi_2^{\mathrm{eff}}}{n(\Omega)c}\frac{\left[e^{i\Delta kz} - e^{-\alpha(\Omega)z/2}\right]}{(\alpha(\Omega)/2 + i\Delta k)} \tag{1}$$

$$\Delta k = \frac{\Omega\left[n(\Omega) - n_{\mathrm{g}}(\omega_0)\right]}{c} - \frac{2\pi}{\Lambda}, \tag{2}$$

where $A_{opt}$ is the combined optical field of the input chirped pulse-train with individual pulses centered at $\omega_0$ and $\mathcal{F}$ denotes the Fourier transform. $\Omega$ is the phase-matched THz angular frequency and $\alpha$ is the absorption coefficient of the medium. In Eq. (2), $\Delta k = 0$ is the condition for perfect phase-matching, where $\Lambda$ is the poling period of the nonlinear medium, and $n$ and $n_{\mathrm{g}}$ are respectively the phase and group refractive indices within the medium. If the process is direct phase-matching rather than quasi-phase-matching then the term with $\Lambda$ is removed and $\chi_2^{\mathrm{eff}} \to \chi_2$.

The optical field must contain frequency content at the phase-matched frequency in the medium, which is described properly by this formulation. The frequency content term $\mathcal{F}_{t\to\omega}\left[|A_{\mathrm{opt}}(t)|^2\right]$ and the phase-matching term (the remainder of Eq. (1)) are both peaked in amplitude, so if they do not peak at the same THz frequency then the THz field will be low along with the total THz pulse energy. This is especially true when the phase-matching is narrow-band, which is the case as the length of the quasi-phase-matching medium increases [21]. Because of this, the 'difference frequency content' will be an important concept in this work that essentially determines the suitability of the combined input NIR pump pulses for producing THz at a given frequency. Because the output THz energy is proportional to $|A_{\mathrm{THz}}|^2$, the relevant optical property for THz energy is $\left|\mathcal{F}_{t\to\omega}\left[|A_{\mathrm{opt}}(t)|^2\right]\right|^2$, which will be referred to as the 'difference frequency content' of the pump pulse-train henceforth.

When the optical field is composed of chirped-and-delayed pulses having a group-delay dispersion (GDD) $\phi_2$ (corresponding to a chirp-rate $1/\phi_2$) separated in time by a delay $\Delta t$, the

Optics EXPRESS

frequency content is peaked at a difference-frequency of $\Delta t/\phi_2$. This produces the important result of an optimum temporal spacing $\Delta t_{\text{opt}} = \Omega\phi_2$ to be matched to the desired frequency $\Omega$ [20]. An important additional condition not reflected directly in the equations here, but only indirectly within the difference frequency content term, is that the optical pump pulses must have significant bandwidth in order to have enough total overlap in time at the optimum delay. Since the chirped NIR pulse duration $\tau_{\text{L}}$ is fixed by the chirp rate and optical bandwidth $\delta\omega_L$ ($\tau_{\text{L}} = \delta\omega_{\text{L}}\phi_2$), there is a lower limit on the optical bandwidth for efficient DFG. For significant temporal overlap $\tau_{\text{L}} \gg \Delta t_{\text{opt}}$ must be satisfied and therefore $\delta\omega_{\text{L}} \gg \Omega$ is a condition for the optical bandwidth.

The requirements for optimum THz generation become much more complex when the overlapped pulses have a nonlinear chirp. A chirped pulse with third-order spectral phase can be approximated as having a Gaussian envelope with a temporal phase $\varphi(t)$ having higher-order terms [19,22–28]. Rather than relying on numerical methods the instantaneous frequency $\omega(t) = -d\varphi(t)/dt$ of a significantly stretched pulse can be written as

$$\omega(t) = \omega_0 + \frac{1}{\phi_2}t + \frac{-\phi_3}{2\phi_2^3}t^2, \tag{3}$$

where $\phi_3$ is the third-order dispersion (TOD). The following section will describe more completely the implications of this, depending on the number of pulses in the pulse-train and the magnitude of the matched frequency $\Omega$.

The THz output depends strongly on the properties of the nonlinear material and how they depend on frequency. This can be isolated by the phase-matching term in Eq. (1), that is, the part of the equation that is not the difference frequency content of the pump pulses. The THz energy is proportional to $n(\Omega)|A_{\text{THz}}|^2$, so the relevant term that depends only on material parameters ($n(\Omega)$, $\alpha(\Omega)$, crystal length $L$) is

$$\eta_{\text{rel}}^{\text{mat}} \propto n(\Omega)\left|\frac{\Omega}{n(\Omega)}\frac{\left[e^{i\Delta kL} - e^{-\alpha(\Omega)L/2}\right]}{(\alpha(\Omega) + 2i\Delta k)}\right|^2, \tag{4}$$

where $\Delta k$ is as before, assuming the pump wavelength is fixed. This can be thought of as the relative efficiency due only to material properties, which we write as $\eta_{\text{rel}}^{\text{mat}}$, or equivalently as an acceptance function for the chosen nonlinear sample of known properties and dimensions [29]. In other words, this phase-matching terms defines the acceptance bandwidth of the nonlinear medium independent of the pump properties.

A ubiquitous property in nonlinear crystals is an increase in absorption as the frequency increases approaching a phonon resonance. These absorption peaks limit the ability of a given material to either produce narrowband THz across a broad tunable frequency band, or limit the ability to produce the broad spectrum necessary for single-cycle THz if that is the desired application. Materials such as ZnTe [30–32], GaAs [33], GaP [34], GaSe [35,36], BBO [37,38], and organic salt crystals [39,40] have been used to produce mid-infrared (MIR) or THz radiation via DFG. Due to varying material properties at both the pump and signal wavelengths, the different desired signal properties require significantly varied experimental parameters and therefore play a part in choosing the nonlinear material. Lithium niobate is used in this work due to its relevance to THz-based acceleration, having a significantly increasing absorption above 1 THz and therefore most suited for sub-THz frequencies [41,42].

The equations in this section as well as the concept of the optical difference frequency content, and the behavior of the THz output only due to material properties are very important to understanding scaling of THz generation via chirp-and-delay. These equations however do not include effects on the spectrum of the NIR pulse-train as THz is generated, which is present in interactions at high efficiency due to cascading of the nonlinear process [14,18,43]. This means that quantitative results are most precise at low efficiencies, but still inform the process in general.

Optics EXPRESS

## 3. Effect of the TOD on input field

The significantly different temporal phase and resulting instantaneous frequency when a pulse has TOD, as in Eq. (3), has a dramatic effect on the available difference frequency content for THz generation. We will analyze this effect quantitatively using experimentally relevant spectral phase values and specific pulse-train formats. The most simple format is two pulses of equal amplitude separated by $\Delta t$. This can be realized, for example, by using a Mach-Zehnder type interferometer. In Ahr et al. [18], a pulse train was produced using a using a high-reflector (HR) and partial-reflector (PR) pair. This etalon configuration forms a pulse-train of an infinite number of pulses with varying amplitudes, still with a constant $\Delta t$ between successive pulses. This was done because it was more practical experimentally, but also because this method uses all of the available laser energy, whereas an interferometer that produces only two pulse copies will have two separate outputs each with 50 % of the laser energy.

The spectral phase values used in the following will always be representative of the pulses produced in the Ti:Sapphire Joule-class Angus laser system, which was the driver for the results of Ahr et al. [18] and Jolly et al. [19], in this case GDD of 2.3 $ps^2$ and TOD of −0.0044 $ps^3$, on pulses having a bandwidth of 35 nm centered at roughly 800 nm. In the following paragraphs we will analyze the consequences of TOD on the DFG content of such pulse trains.

When creating such a train of pulses as in Ahr et al. [18] a PR with R=38 % and a HR with 100 % reflectivity are used. There is a theoretically infinite train of pulses with the energies $E_1 = R, E_n = R^{n-2}(1-R)^2$, with the first two pulses having approximately equal energy of 38 % of the total, with the energy decreasing in pulses thereafter. The total optical field can be written as a sum of this pulse train:

$$A_{\text{opt}}(t) = \sum_{n=1}^{\infty} E_n A_n(t-(n-1)\Delta t) \tag{5}$$

$$A_n(t) \propto \exp\left[\frac{-2\ln(2)t^2}{(\delta\omega \text{L}\phi_2)^2}\right] \exp\left[-i(\omega_0 t + \frac{t^2}{2\phi_2} + \frac{-\phi_3 t^3}{6\phi_2^3})\right]. \tag{6}$$

This description of the field produces a much different picture of the input IR energy than analysis using only GDD, or only a pair of pulses. Because there is TOD, i.e. a curved frequency across the pulses in time, and in the case of the infinite pulse train many pulses overlapping, there is now complex temporal interference which includes even an effect on the overall envelope of the IR energy. The significance of the effect of TOD and a larger pulse train can be seen in the changes on the field of the delayed and overlapped pulses $|A_{\text{opt}}(t)|^2$, and on the difference frequency content available for producing THz defined as $|\mathcal{F}_{t\to\omega}[|A_{\text{opt}}(t)|^2]|^2$.

To illustrate these effects we show in Fig. 2 the combined optical field and the difference frequency content for a pulse train of $N$=2 and $N$=10 pulses, where $N$ is a finite limit in the sum of Eq. (5). Here we assume a temporal delay of 5.78 ps, in order to produce 400 GHz radiation with the assumed GDD of 2.3 $ps^2$ on the pump pulses.

As shown in Fig. 2, the overall envelope of the overlapped pulses is largely unchanged when there is no TOD or no pulse train (Figs. 2(a)–2(c)), except with both TOD and the longer pulse-train (Fig. 2(d)). In that last case the envelope becomes significantly more complex, and also has a larger peak field due to the more complex temporal interference.

Looking at the substructure within the overlapped field intensity $|A_{\text{opt}}(t)|^2$ reveals the more complete picture, shown in the insets in Figs. 2(a)–2(d). In the case without the TOD or the pulse train, the sub-pulses due to the beating are regular and at one frequency. When TOD is introduced, the sub-pulses are still regular, but vary in frequency over time. When the pulse-train is included the sub-pulses are no longer regular, indicating the presence of harmonics. Although these effects on the envelope are somewhat instructive, it is only the difference frequency content that has a direct consequence on the DFG process.

Optics EXPRESS

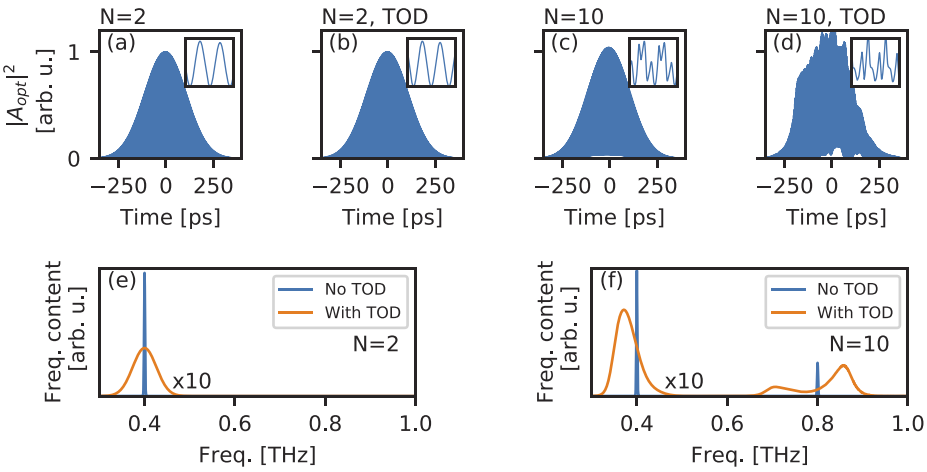


**Fig. 2.** Comparison of the total pulse train envelope (a-d) and frequency content (e-f) for a pulse train of $N$=2 and $N$=10 pulses and drive pulses with and without TOD. In this specific example the THz frequency is centered at 400 GHz with pulses (GDD=2.3 ps$^2$, TOD=-0.0044 ps$^3$) delayed by $\Delta t$=5.78 ps. Insets in panel (a-d) show a zoom from 150-156 ps which captures the temporal interfences responsible for the difference frequency content.

The difference frequency content is sharply peaked when the TOD is zero (Fig. 2(e)) regardless of the number of pulses, which is equivalent to saying that across the envelope the instantaneous difference frequency does not vary significantly (or equivalently that the spacing of the sub-pulses does not change). In the case with zero TOD and a train of ten pulses, there are higher harmonics present in the frequency content. This is because in this case there is still significant overlap between the first and third pulse, or second and fourth, etc. (only the first higher frequency peak is shown). Because the overlap is less complete and the energy in the N>3 pulses is significantly lower than the first and second, the frequency content in these harmonics is also usually much lower than that in the principal.

When the TOD of $-0.0044\,\text{ps}^3$ is included however (Fig. 2(f)), the difference frequency content is no longer as sharply peaked. With only two pulses and TOD the peak of the frequency content is more than an order of magnitude lower and wider than the case without TOD. This is a consequence of the difference frequency varying significantly across the overlapped pulses. In the case with a longer train of ten pulses and also a finite TOD, the frequency content gets similarly more complex as did the envelope. This is due to the intricate temporal interference between all number of pulses.

It is instructive to another level to view this increased complexity in the difference frequency content at various temporal delays (equivalently different generated THz frequencies). Figure 3 shows the same permutations of number of pulses ($N$=2, $N$=10) and TOD (0 ps$^3$, $-0.0044$ ps$^3$) at the original delay of $\Delta t$=5.78 ps, and an additional three delays of 2.89, 8.67, and 11.56 ps that would produce 200, 600, and 800 GHz radiation respectively. The broadening and decrease of the frequency content is present in all cases. However, the complexity of the difference frequency content with $N$=10 (peaks and valleys, asymmetric broadening) increases with the temporal delay (and therefore also with the generated THz frequency). This is a result of the increase in the difference between overlapping frequency components as the temporal delay increases. When the time between each pulse in the train increases, at any given point in time there is a larger and more disparate set of frequencies overlapping with an increasingly different amplitude.

The result of this analysis is that the presence of TOD on the chirped pulses used to create a pulse-train will decrease the peak available frequency content for the DFG process. If the driving

Optics EXPRESS

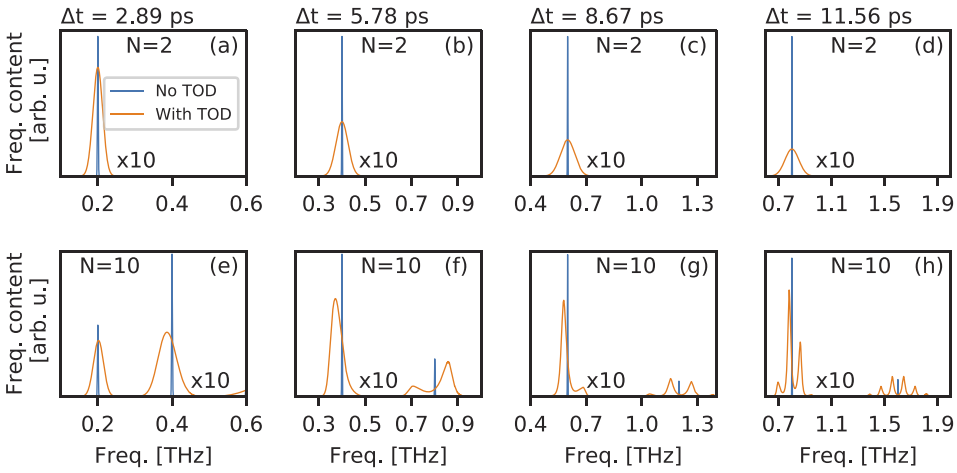


**Fig. 3.** Comparison of the total pulse train difference frequency content at many time delays. We show the same permutations of no TOD (blue) and a TOD of $-0.0044\,\mathrm{ps}^3$ (orange), $N$=2 pulses (a)–(d) and a pulse train ($N$=10) (e)–(h), at the four different delays $\Delta t$=2.89, 5.78, 8.67,11.56 ps necessary to produce frequency content centered on 200, 400, 600, and 800 GHz respectively. Panels (b) and (f) are a duplication of Figs. 2(e) and 2(f).

pulse-train is more complex than just two pulses of the same energy, then increased complexity occurs as well. The following sections will show some experimental nuances resulting from these physics, verifying the conclusion, along with some supporting theoretical explanations.

## 4. Signature of TOD in experimental data

The presence of TOD has a significant effect on the DFG process via its impact on the available difference frequency content, as shown in the previous sections. In the following sections experimental results verify this, and some of the nuances of this effect are expanded upon. Past experiments using an infinite train of broadband chirped pulses in PPLN [18] showed the viability to produce high-energy (tens of $\mu$J) THz pulses in the 0.5 THz range. These results already had a relatively high IR-to-THz 'internal efficiency' of 0.13 % (defined as the efficiency within the crystal, neglecting Fresnel losses for both the IR at the input and the THz at the output). Along with these results the work also showed the expected dependence of the optimum temporal delay and output THz frequency on the parameters of the PPLN, and the increase in efficiency when the crystal was cooled to cryogenic temperatures (which reduces the THz absorption).

The experimental apparatus used for these past results and the results presented here is reproduced in Fig. 4. The driver laser is the Ti:Sapphire-based Angus laser system, with relevant temporal properties the same as those already used in the previous section. The pulse-train is created with a PR/HR combination to produce two equal pulses and a train of lower energy pulses, with the spacing between each subsequent pulse a constant $\Delta t$. The beam is resized to fit approximately the aperture of a given crystal using cylindrical lenses, and the THz is collected using a pair of off-axis parabolic mirrors (OAPs) on to a pyroelectric detector (Gentec-EO: THZ9B-BL-BNC). In the case of the crystal with 330 $\mu$m poling period there are no lenses used to demagnify the pump beam, and a single TPX lens is used to focus the THz beam onto the pyroelectric detector. A longitudinal interferometer was used to measure the center frequency in the case of the two crystals with the highest THz output. The output IR energy is dumped on a sheet of Teflon, and the spectrum of that scattered output is measured with a combination of a diffuser and a fiber spectrometer. The input IR spectrum is recorded automatically with the laser

Optics EXPRESS

controls system. The crystal is contained within a small vacuum chamber to allow for cryogenic cooling to roughly 80 K.

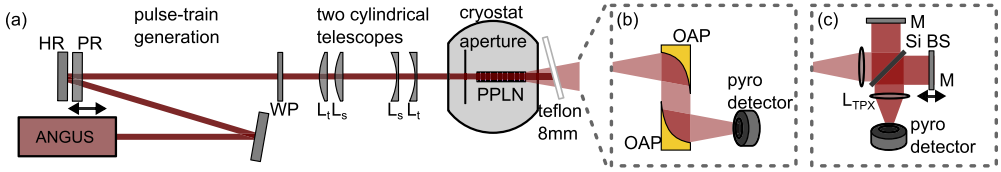


**Fig. 4.** Chirp-and-delay experimental setup (a), identical to the previous work in Ahr et al. [18]. This HR-PR combination produces a train of pulses rather than two pulses of equal energy. A waveplate is used to match perfectly the polarization of the IR light to the PPLN crystal axis. The beam is matched to the aperture of the PPLN crystal using a telescope, the parameters of which depend on the PPLN aperture. A Teflon plate separates the drive laser from the generated THz at the output of the crystal, whose energy is detector using a pyroelectric detector (b). The frequency of the generated THz is verified using an interferometer (c).

Results from Ahr et al. [18] will now be revisited with the TOD analysis in mind, and effects will be elucidated using additional complementary measurements not previously shown.

### *4.1. Modifications of the pump spectrum by THz generation*

The measured output pump spectrum shows significant red-shifting due to the THz generation process (Fig. 5(a)). This is due to, in the case of highly efficient generation, the cascading of the DFG process whereby IR photons take part in the frequency down-conversion process multiple times [43]. Equivalently, the pump spectrum must change as the IR photons are shifted many times. This is easy to imagine in the case of a narrow-band pump [44], but in the case of a broadband pump the cascaded IR remains within the original bandwidth. However, it can be seen that especially at low fluence, but even still at high fluence, the shifting of the IR spectrum does not take place across the whole spectrum (Fig. 5(b)). This dip in the spectrum is a signature of the THz generation process not being phase-matched at every point in time across the individual chirped pulses in the pulse train (and therefore also spectrum, since the the chirp of the pulses relates spectrum and time).

It is possible using the simple temporal phase relation already derived to show that the dip is a direct consequence of the TOD. Since one can write the instantaneous frequency analytically as in Eq. (3), the difference frequency at a delay $\Delta t$ can also be written when the overlapped pulses are assumed to be copies of each other:

$$\Delta\omega(t) = \left[\frac{\Delta t}{\phi_2} + \frac{\phi_3 \Delta t^2}{2(\phi_2)^3}\right] + \left[-\frac{\phi_3 \Delta t}{(\phi_2)^3}\right] t. \tag{7}$$

With pulses that are not copies of each other, such as in [36,40,45] for example, this relationship becomes much more complex (and only applies if the chirp is large). This difference frequency is now in any case not constant with time, which was already shown schematically in Fig. 1(b) when introducing the concept.

If the expected THz frequency $\Omega = 2\pi\nu_{\mathrm{THz}}$ is known, then it can be calculated which part of the delayed and overlapped pulses will be beating at that frequency at the time delay $\Delta t$. For this analysis only two pulses will be assumed, since they contain the majority of the total pump energy. Fixing the difference frequency from Eq. (7) to exactly the frequency of the generated

Optics EXPRESS

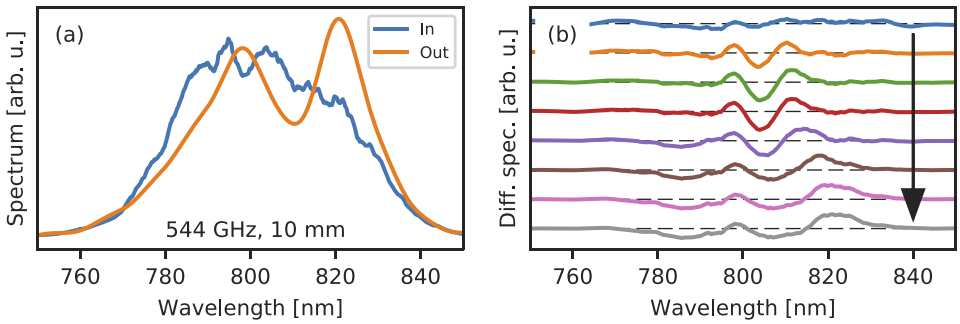


**Fig. 5.** Effect of THz generation on the IR spectrum. (a) Comparison of the input and output spectrum of the main drive laser. The conversion of IR photons to THz causes a redshift of the spectrum, but there is a distinct 'dip' that only occurs in a small region. (b) The difference between the input and output drive spectrum shows prominent signatures of cascading, i.e. the multiple frequency down-conversion of the IR drive photons, as the input fluence increases and the conversion to THz becomes more efficient and the 'dip' becomes wider. The difference is shown for fluence levels in the range from 43 to 600 mJ/cm$^2$ with the arrow pointing towards increasing fluence. All data use a 544 GHz crystal (212 $\mu$m poling period) of 10 mm length.

THz as follows

$$\Omega = \frac{\Delta t}{\phi_2} + \frac{-\phi_3}{2\phi_2^3}\left(t_{\text{gen}}^2 - (t_{\text{gen}} - \Delta t)^2\right) \tag{8}$$

fixes as well where the THz at exactly that frequency is being produced within the pump pulses. At a given delay there is a time $t_{\text{gen}}$ where the THz at $\Omega$ is being produced relative to the peak of the first pulse

$$t_{\text{gen}} = \frac{\Delta t}{2} + \frac{\phi_2^3}{\phi_3}\left[\frac{1}{\phi_2} - \frac{\Omega}{\Delta t}\right]. \tag{9}$$

In the second pulse the THz is being produced at a time $(t_{\text{gen}} - \Delta t)$ relative to the peak of that pulse.

Since the relationship between time and frequency is already known (simply the instantaneous frequency $\omega(t)$ in Eq. (3)) then the portion of the *spectrum* responsible for the THz production can be calculated based on $t_{\text{gen}}$. Since the first and second pulse have equal energies (again, ignoring in this case lower energy pulses in the pulse-train) then the spectral content producing the THz most efficiently is

$$\omega_{\text{avg}} = \frac{\omega(t_{\text{gen}}) + \omega(t_{\text{gen}} - \Delta t)}{2} = \omega_0 + \frac{\phi_2}{2\phi_3} - \frac{\Omega^2\phi_2^3}{2\Delta t^2\phi_3} - \frac{\Delta t^2\phi_3}{8\phi_2^3}, \tag{10}$$

which is the average frequency in the combined IR pump pulses. One can then convert to wavelength, $\lambda_{\text{avg}} = 2\pi c/\omega_{\text{avg}}$, and compare directly to the measured experimental data. Figure 6 illustrates the effect of different parts of the spectrum contributing to THz generation as the delay between the pulses varies. We show measured data from 4 different crystals with different poling periods, generating THz at 300 GHz, 350 GHz, 544 GHz and 860 GHz. As the temporal delay is changed in the four different cases, the spectral location of the 'dip' moves across the pump spectrum. This location in the spectrum fits remarkably well with the $\lambda_{\text{avg}}$ calculated above, shown in the white lines of Fig. 6. This is direct experimental evidence of the incomplete and varying participation of the pump spectrum in the DFG process due to the presence of TOD.

Optics EXPRESS

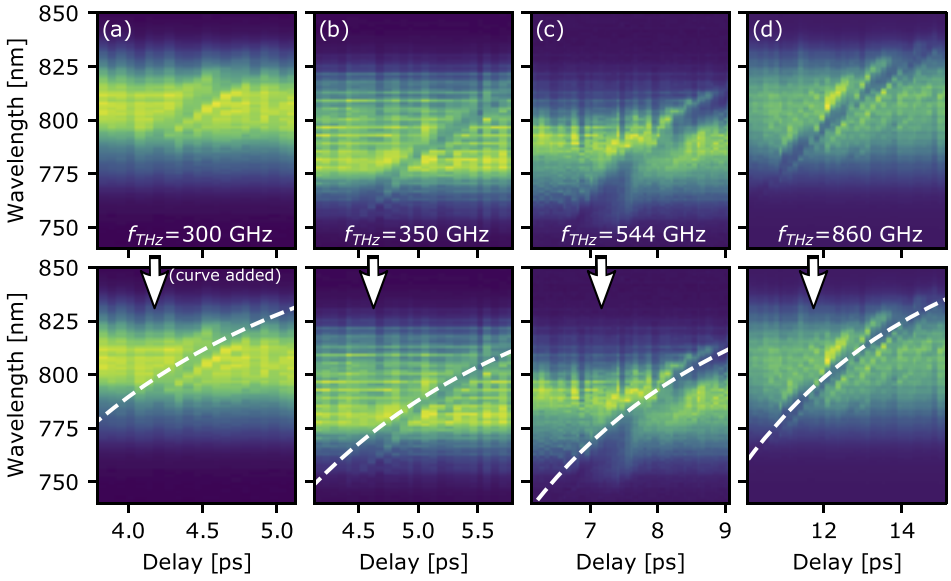


**Fig. 6.** Experimental output IR spectrum during a delay scan of a train of IR pulses generating THz in four different poling period PPLN crystals producing four different frequencies of (a) 300 GHz, (b) 350 GHz, (c) 544 GHz, (d) 860 GHz. As the delay between the pulses varies, different parts of the drive spectrum contribute to THz generation, which manifests as a moving local dip in spectral intensity shown clearly in the top row. The experimental data matches very well with our predicted behavior (white line added on the bottom row, from Eq. (10)). Pump fluence is low (below 100 mJ/cm$^2$) in all cases so that the dip is localized.

### *4.2. THz generation efficiency as a function of delay*

This section shows the expected behavior of THz output as a function of temporal delay in the PPLN, and shows that the observed complexity can only be predicted when including both TOD and the entire pulse train, confirming another experimental result that is directly caused by the TOD.

The THz output can be calculated according to Eq. (1) using the calculated difference frequency content via an FFT of the optical field to frequency space. The most simple expected behavior is that as the temporal delay sweeps over the predicted optimum ($\Delta t_{\text{opt}} = \phi_2\Omega$) the THz output peaks. This corresponds to the delay where the largest amount of the difference frequency content is within the QPM bandwidth. This was observed experimentally in Ahr et al. [18] and behaved essentially as expected when using crystals of different poling periods (producing different frequencies). However, in more than one case the output as a function of delay was not as simple as a single peak. The increase in complexity of the envelope and frequency content shown in Section 3 already provides a hint at the behavior of the THz output as a function of delay, since the THz energy is related to this complex frequency content, but only within the bandwidth of the process.

Figure 7 shows the measured THz (with arbitrary vertical scale) as a function of delay for the two cases with the most complexity (also the two highest frequencies), crystals of poling perdiod 212 and 125 $\mu$m producing 544 and 860 GHz respectively. Calculations (Figs. 7(b) and 7(e)) are similar to the qualitative behavior of the frequency content. The THz output as a function of delay is sharply peaked when no TOD is present. When TOD is present, but the calculation is still only with two pulses, the output is lower and spread over a wider range of delays. However, only when

Optics EXPRESS

both the TOD and pulse train are included in the calculations can the observed complexity on the delay behavior be reproduced (i.e. the multiple peaks seen in Figs. 7(a) and 7(d)). Although the experimental curves do not exactly match with the FFT+analytic calculations, the agreement is remarkably good qualitatively. This observation can be linked back to Section 3 by noting the similarity between the calculations with TOD and a pulse train and the experimental results in Fig. 7 with the frequency content shown in Figs. 3(g) and 3(h).

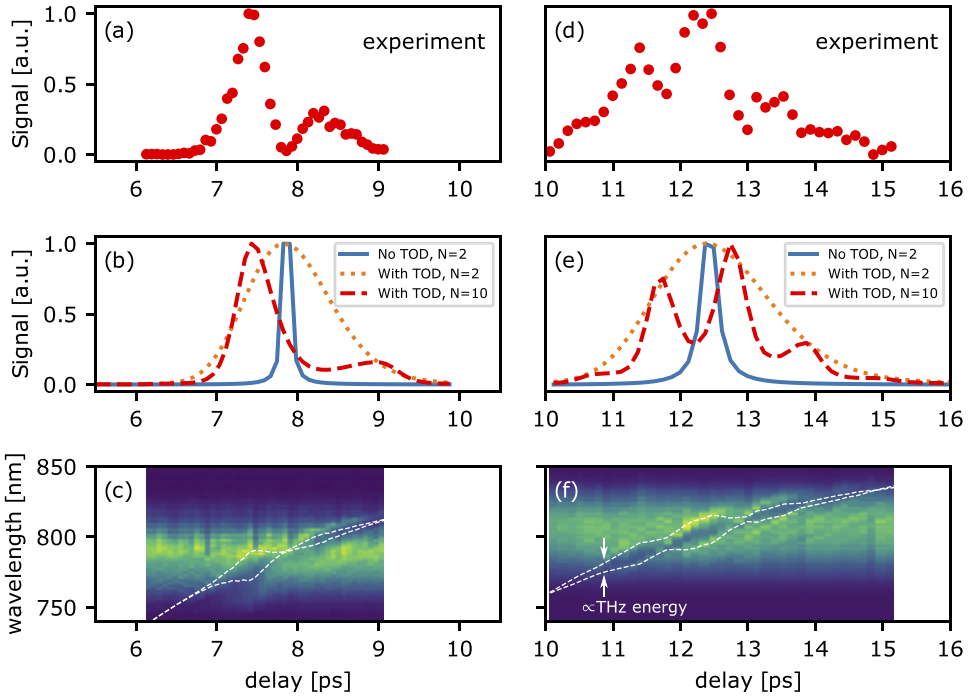


**Fig. 7.** Comparison of the measured THz output energy at different temporal delays (a) and (d), and that by calculating (c) and (e) the expected output of the THz generation process at each time delay with two fixed PPLN crystal properties (crystals of poling perdiod 212 and 125 $\mu$m producing 544 and 860 GHz respectively). The calculation includes permutations of no TOD and realistic TOD, 2 pulses and a pulse train. The width of the delay scan increases when TOD is included, but the complexity seen in experiments ((a) and (c)) is only visible when including the whole pulse train (dashed red lines). The complexity seen in the IR output spectrum in both cases can be explained by an increase in the spectral dip width proportional to the generated THz, shown in (c) and (f).

The spacing between the peaks and dips in the THz output as a function of delay is related to the inverse of the THz frequency in each case (1.84 ps and 1.16 ps spacing for the 544 GHz and 860 GHz results respectively). This is due to the interference between the THz generated between pulse 1 and 2, and pulse 2 and 3, etc., which are always at the same frequency, but separated in time by the varying delay. This predicted separation of the peaks is exactly shown in the calculations, but is only approximately present in the experimental results. This understanding is physically equivalent to the previous explanation based on the difference frequency content.

The agreement extends also to the 'dip' seen in the output IR spectrum, which increases in width based on the amount of generated THz. Two white lines are shown in Fig. 7(c) and 7(f), which have a central location based on Eq. (10) and a separation proportional to the experimentally measured THz energy, showing very good agreement with experimental spectral data (see Fig. 6 for unobstructed spectra).

Optics EXPRESS

## 5. Effect of TOD on efficiency of THz generation via quasi-phase-matching

It was shown so far that the inclusion of TOD in the DFG process vastly changes the specifics of the interaction between the overlapped pulses in the pulse-train and therefore also the generation of the lower frequency THz radiation. The inclusion of TOD in analyses showed that the THz is only generated from a certain portion of the input pump spectrum, and that when including the entire pulse-train present in experiments, previously uncharacterized features can be explained. However, it is most important for applications requiring very high THz energies that the efficiency of the process remains high and therefore more of the total pump pulse energy can take part in the THz generation.

What was shown in an earlier section is that the peak available difference frequency content decreases when TOD is present. If the THz generation process were infinitely broadband then this would have no effect on total THz energy, but when narrowband THz pulses are being produced within cm-long PPLN crystals the relative bandwidth of the process becomes very narrow. Therefore this decrease of the peak frequency content also results in a decrease of the output THz energy. We use the modelled fields as in Eq. (6) and the QPM in Eq. (1), and integrate over frequency to calculate the expected THz output (and therefore THz generation efficiency) at various frequencies and lengths in PPLN.

We calculate the decrease of THz output for different phase matching bandwidths. As we use PPLNs of different frequency (poling period) and crystal length, this changes the number of PPLN periods and thus the phase matching bandwidth of the crystal. In Fig. 8 we show calculation for two crystals at 360 and 720 GHz frequency, and lengths of 0.5, 1.0, 2.0, and 3.6 cm using PPLN material properties and the Angus parameters. As TOD is increased, output THz is significantly decreased at every length, by more than an order of magntiude in some cases. This decrease is more severe the longer the crystal, which corresponds to THz with a narrower bandwidth. The relative decrease in THz output is also greater at higher frequencies where the relative bandwidth is narrower at a fixed length.

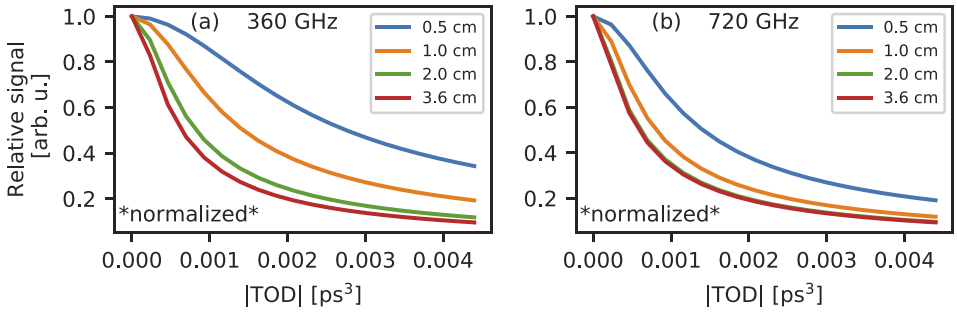


**Fig. 8.** The relative decrease in THz generation efficiency due to TOD for different frequencies and lengths with the Angus pump parameters in PPLN. In all cases as the TOD increases the efficiency drops monotonically relative to the case with zero TOD. Calculations are made with the FFT+analytic method using Eq. (1) and therefore do not take in to account nonlinear cascading. Shown are results for 360 GHz (a) and 720 GHz (b) at lengths of 0.5, 1.0, 2.0, and 3.6 cm.

Of course as the crystal is longer, although the relative decrease in efficient due to TOD is stronger, the process has more length over which the THz output increases. So in the analytic model used the total output increases with length with every amount of TOD, at any frequency. However, since this analysis does not take in to account any saturation of the process, this cannot be true as the crystal length increases indefinitely or as the fluence is increased.

Optics EXPRESS

We have recently shown compensation for this effect on efficiency via asymmetric addition of GDD and TOD to the pump pulses, producing mJ-level pulses with 1 % bandwidth at 361 GHz [19], confirming that the TOD does indeed have a significant effect on THz generation efficency. The results in Jolly et al. [19] showed an increase by a factor of 13 when compensating for the effect of the TOD in a 3.6 cm long crystal producing 361 GHz radiation, which agrees well with the red curve in Fig. 8(a) for the experimental TOD value of $-0.004\,\mathrm{ps}^3$ in that case.

## 6. Generation of temporally complex THz pulses

The results shown in Section 4 of complex behavior of the THz output on time delay was interpreted via the difference frequency content shown in Section 3. This can be interpreted as well as a signature of the temporally multiplexed generation of THz, i.e. production of THz at distinct moments in time, which has the potential to be engineered to produce more complex temporal profiles or even distinct THz pulses separated in time.

The original scheme of the previous sections is shown in Fig. 9(a), where there is a train of pulses produced from the HR/PR pair. These pulses are all copies of each other with a varying energy, excluding the negligible material dispersion of the partial reflector. The difference frequency between each adjacent pulse pair has a significant slope as derived already in Eq. (7). The combination of the slope of the instantaneous difference frequency and the pulse train results in more than one moment in time within the phase-matching bandwidth at a given delay. These distinct moments in time are denoted as 'THz 1' and 'THz 2' in Fig. 9(b), corresponding to the matched difference-frequency between pulse 1 and pulse 2, and pulse 2 and pulse 3, respectively.

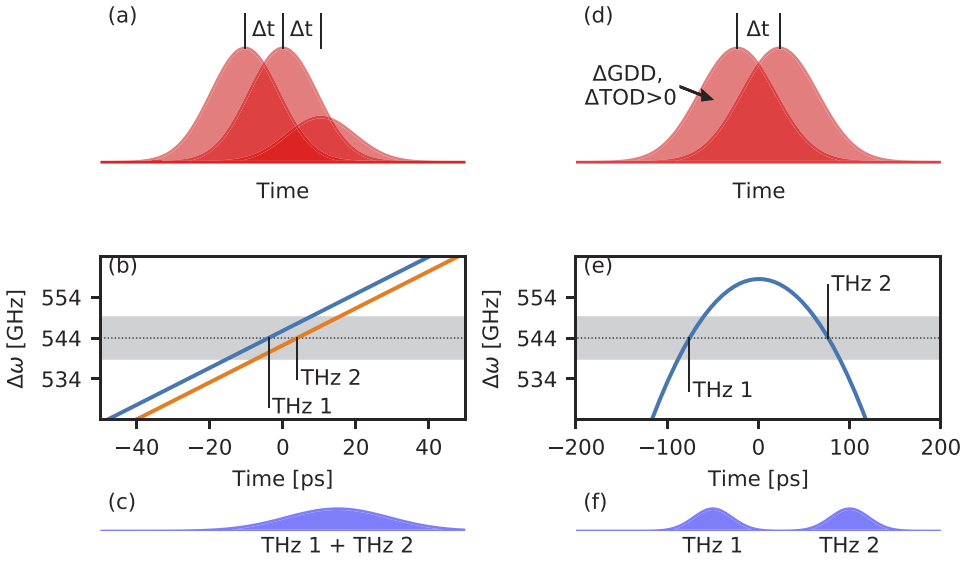


**Fig. 9.** The production of temporally complex THz pulses. (a), a train of identical pulses with varying energy, shown with only pulses 1–3 and (b), the instantaneous difference frequency between pulse 1 and pulse 2 (blue), and pulse 2 and pulse 3 (orange). Due to this input pulse format THz is generated at two distinct moments in time, denoted as 'THz 1' and 'THz 2'. At the proper delay this still results in only one output THz pulse, shown in (c). (d), a pair of pulses could be engineered with additional ΔGDD and ΔTOD added to only one pulse ($15500\,\mathrm{fs}^2$ and $300000\,\mathrm{fs}^3$ respectively) such that isolated THz pulses are generated at moments in time that are far apart, as shown in (e). In (f) we show the output THz, which now is two distinctly separated pulses. The duration of the THz pulses depends on many experimental parameters (see text).

Optics EXPRESS

The complex delay scans shown earlier in Figs. 7(a) and 7(b) are essentially a result of the interference between the THz generated at these two (or more) points in time, where still only one final THz pulse is generated as in Fig. 9(c).

Pushing this concept of temporally-multiplexed THz generation further, pump pulses could be manipulated separately (for example as in Jolly et al. [19] in a Mach-Zehnder setup) to have a specific slope and curvature of difference frequency so that THz pulses are generated at a designed temporal separation. An example is shown in Figs. 9(d)–9(f) to have only a quadratic component of difference frequency resulting from positive $\Delta\phi_2$ and $\Delta\phi_3$ on only the first pulse. There is phase-matching at two points in time with a separation of about 150 ps.

It is important to note that the longer the crystal the larger an effect group-velocity walk-off will have on the temporally separated THz pulses, causing the THz to extend from the position in time it is initially generated relative to the NIR pump pulses. The pulse duration of the pump also plays a role, since the temporal extent of the THz from a single phase-matching point depends on both the crystal length and pump pulse duration (and indeed the absorption of the crystal) [46]. Closely separated phase-matching points (Fig. 9(b)) produce a single THz pulse with possible temporal structure (Fig. 9(c)), and widely separated phase-matching points (Fig. 9(e)) produce two separate THz pulses (Fig. 9(f)), with the intermediate scenarios producing terahertz with two peaks. The experimental results from the HR/PR setup correspond to the former situation, where the two distinct phase-matching regions overlap significantly in time. So-called double-peak THz pulses may have interesting applications to highly controlled particle manipulation, or to specific delayed resonant pumping of materials.

This discussion is inherently related to the generation of broadband DFG in aperiodically poled crystals [47,48], but that is beyond the scope of this article.

## 7. Discussion of the effect on chirp of THz pulses

Outside of effects on the temporal envelope of the THz, it is also possible that the TOD imparts a chirp on the THz pulses. However, in the case of quasi-phase-matching in long PPLN crystals the narrowband nature of the phase-matching bandwidth allows for production of terahertz only at that very small range of frequencies. Taking into account that pulse duration is significantly determined by the crystal length and not only the temporal extent of the phase-matched pump pulses (i.e. the dispersive nature of the process), then the chirp in this case must be small.

If the THz generation process is broadband and the dispersion is not significant (for example in a thin nonlinear crystal), then the chirp on the THz would be related directly to the linear term in the instantaneous angular frequency of the overlapped optical pulses $-\phi_3\Delta t/\phi_2^3$ derived earlier when $\Delta t = \phi_2\Omega$. The THz chirp $b_{\mathrm{THz}}$ will be defined as the derivative of the instantaneous frequency of the THz such that

$$\nu_{\mathrm{THz}}(t) = \nu_{0,\mathrm{THz}} + b_{\mathrm{THz}}t + \ldots. \tag{11}$$

So in a case such as this, without a limitation to the bandwidth, the chirp on the THz pulses would be $b_{\mathrm{THz}} = -\phi_3\nu_{\mathrm{THz}}/\phi_2^2$, similar to that derived in previous work [25]. Therefore, if the chirped and delayed pulses are *copies* of each other and have TOD, the chirp must be expected or steps must be taken to remove it, for example by a second grating compressor for the pump beam [26] or the aforementioned asymmetric tuning of the pump spectral phase [19]. Note that the higher the phase-matched frequency is the larger the chirp.

There may also be significant chirp present if the pulses are not exact copies, with a more complex description necessary [19]. In some examples of chirp-and-delay in thin nonlinear crystals in the literature [36,40] they used two separate OPAs that had specifically tuned GDD and TOD in order to produce THz and MIR pulses that have negligible chirp at the very small temporal delays used. In other examples [32,39] the THz chirp may be relevant depending on the level of GDD and TOD in the pump beams. This is in contrast to the demonstrated pulse shaping

Optics EXPRESS

in the MIR via DFG [49,50] where the chirp in the DFG radiation was caused by pulses with different GDD (and central wavelength), and TOD was not taken in to account.

If the broadband pulse copies from Angus were used in a crystal such as GaP, then one would match the delay to a frequency band with low enough absorption and good enough phase-matching, for example around 7.17 THz. The produced narrowband radiation would have roughly the spectral envelope of the entire difference frequency content, and a chirp corresponding to that derived in this section. This is shown in Fig. 10, with Angus pulses at $\Delta t$ = 103.75 ps for a 0.5 mm thick GaP.

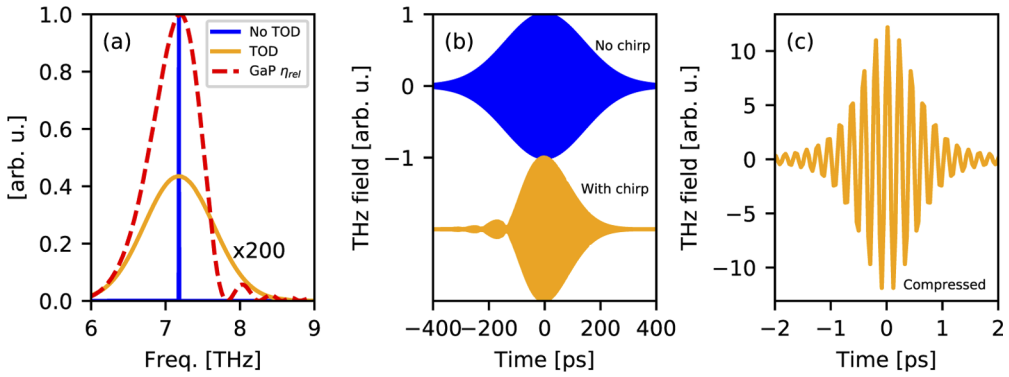


**Fig. 10.** Producing chirped THz pulses via broadband direct phase matching. The frequency content (a) of Angus pulses with $\Delta t$ = 103.75 ps (matched for 7.179 THz) with and without TOD (solid), overlaid with the $\eta_{\mathrm{rel}}$ for 0.5 mm GaP (dashed). The peak without TOD is so narrow so as to not be visible. The THz pulses produced (b) with TOD (orange) and without TOD (blue) on the pump pulses, that have either a linear chirp or flat phase respectively. If the chirped pulse were compressed (c) the temporal envelope would correspond to the Fourier-limit of the broad bandwidth of the frequency content and GaP phase-matching.

In the case of the Angus parameters, the difference frequency content when no TOD is present (Fig. 10(a)) has an extremely narrow bandwidth of 0.04 % FWHM, contrary to the much larger bandwidth when TOD is present. In this case of direct phase-matching in a short crystal, contrary to quasi-phase-matching in long crystals, the bandwidth of the THz depends almost entirely on the pump pulses and only indirectly depends on the crystal length via the $\eta_{\mathrm{rel}}$ for 0.5 mm GaP. The THz spectrum, either with or without TOD on the pump pulses, is related to the product of the difference frequency content and $\eta_{\mathrm{rel}}$. Therefore, the extreme narrow width is still present on the generated THz, shown in time in Fig. 10(b). The THz produced when TOD is present has a larger bandwidth overall, but the spectral envelope is narrowed due to the limited phase-matching in GaP. The key difference is that this pulse has chirp, which combined with the total spectral envelope produces the pulse in time shown in Fig. 10(b). A method of compensation similar to that used to generate higher efficiencies in Jolly et al. [19] could be used to remove or tune the THz chirp, although in this example at a higher frequency it would be more difficult experimentally. Figure 10(c) shows a THz pulse that would result from compressing the broader, chirped THz pulse produced when TOD is present on the pump. It could be that when driven strongly enough, compressing such pulses could result in very high field strength.

These calculations confirm that using such a pump with TOD would produce significantly different THz pulses via broadband direct phase-matching than when TOD is not taken in to account. However, they also show that if TOD were removed then the generated THz would be remarkably narrowband. From another point of view, varying the TOD on the pump pulses would also produce THz pulses with variable chirp, with a larger dynamic range at higher THz frequencies. These pulses could be either designed to have a certain chirp, or compressed

Optics EXPRESS

to produce higher peak field. This discussion could provide a new path toward tunable THz waveforms, or for producing extremely narrow bandwith THz pulses via chirp-and-delay with highly chirped driving pulses (which generally contain TOD).

## 8. Conclusion

The effect of the TOD has been shown to be especially significant on the generation of THz with trains of chirped pulses. This effect applies for a wide-range of pump pulse properties and nonlinear media. The first conclusion is that TOD changes the difference frequency content of the total pump IR energy, which is due to a varying difference frequency over time within the overlapped train of pulses. When there is additionally a longer train of >2 pulses the combination of TOD and this greater number of pulses adds complexity to the difference frequency content. Both the varying difference frequency and increased complexity were shown via signatures in experimental results from quasi-phase-matching in PPLN driven by the Angus system at sub-THz frequencies.

The TOD effects go even further, as the change in the difference frequency content results as well in a decrease in the efficiency of the THz generation process via quasi-phase-matching. This was predicted to be an effect of over an order of magnitude in the calculations of Section 5 for sub-THz frequencies in cm-scale length PPLN using the analytic description. This effect on efficiency is extremely important for applications requiring high energy narrowband THz, and was independently confirmed in our own recent experiments [19]. We also showed that with certain modifications to the spectral phase, temporally separated THz pulses could be generated via narrowband DFG. Lastly, the effect of the TOD on broadband DFG was shown to be primarily a linear chirp in the produced DFG radiation, with the magnitude of the chirp being directly related to the pump laser properties.

All of the effects touched upon were quantitatively derived for the case of highly-chirped pulse *copies*, but the analysis also applies conceptually to more general cases. Other such cases include using optical parametric amplifiers (OPAs) that are at different central wavelengths (i.e. not pulse copies) where the pulses are either Fourier-limited, broadband [35] or narrowband [44,51,52], or chirped [36–38,40,45,53,54] (named the DC-OPA). In all of these cases TOD would also have a significant effect, but the severity depends highly on the specific parameters. Relevant also for THz and far-infrared generation is intra-pulse DFG where the intrinsic bandwidth of the single driving short pulse provides the difference frequency content [14,55,56], which as well contains a signature of TOD in the driving pulse [29]. It is even related to a more complex interplay between linear and nonlinear effects observed recently [57]. Beyond THz generation via DFG the analysis in this manuscript also has impact on the generation of periodic density modulations in relativistic electron beams [27,58–62] and current modulations in two-color laser-plasma filaments [63] produced via chirped pulse beating, which are pursued with the goal of producing THz radiation via secondary processes.

The manuscript shows that TOD in the driving laser pulses can have very significant effects on critical parameters of the generated THz. These parameters include the total efficiency of the narrowband process, the complexity of the produced narrowband THz pulse envelope, and on the THz temporal phase in the broadband phase-matching scenario. The implications are both on the ability to optimize the process and control the DFG waveform, with a wide range of applications to THz and MIR sources.

## Funding

European Research Council (609920); Bundesministerium für Bildung und Forschung (05K16GU2); Deutsches Elektronen-Synchrotron (Strategy Fund); PIER (PIF-2017-67); European Regional Development Fund (CZ.02.1.01/0.0/0.0/15_008/0000162).

Optics EXPRESS

## Acknowledgments

We thank M. Schnepp and V. Leroux for help with the laser system, and H. Ishizuki and Prof. T. Taira for providing a PPLN crystal with 330 $\mu$m poling period used for the results in Fig. 6(b).

## Disclosures

The authors declare no conflicts of interest.

## References

1. J. Hebling, K. L. Yeh, M. C. Hoffmann, and K. A. Nelson, "High-power THz generation, THz nonlinear optics, and THz nonlinear spectroscopy," IEEE J. Sel. Top. Quantum Electron. **14**(2), 345–353 (2008).
2. L. J. Wong, A. Fallahi, and F. X. Kärtner, "Compact electron acceleration and bunch compression in THz waveguides," Opt. Express **21**(8), 9792–9806 (2013).
3. E. A. Nanni, W. R. Huang, K.-H. Hong, K. Ravi, A. Fallahi, G. Moriena, R. J. D. Miller, and F. X. Kärtner, "Terahertz-driven linear electron acceleration," Nat. Commun. **6**(1), 8486 (2015).
4. F. X. Kärtner, F. Ahr, A.-L. Calendron, H. Çankaya, S. Carbajo, G. Chang, G. Cirmi, K. Dörner, U. Dorda, A. Fallahi, A. Hartin, M. Hemmer, R. Hobbs, Y. Hua, W. R. Huang, R. Letrun, N. Matlis, V. Mazalova, O. D. Mücke, E. Nanni, W. Putnam, K. Ravi, F. Reichert, I. Sarrou, X. Wu, A. Yahaghi, H. Ye, L. Zapata, D. Zhang, C. Zhou, R. J. D. Miller, K. K. Berggren, H. Graafsma, A. Meents, R. W. Assmann, H. N. Chapman, and P. Fromme, "AXSIS: Exploring the frontiers in attosecond X-ray science, imaging and spectroscopy," Nucl. Instrum. Methods Phys. Res., Sect. A **829**, 24–29 (2016).
5. M. Fakhari, A. Fallahi, and F. X. Kärtner, "THz cavities and injectors for compact electron acceleration using laser-driven thz sources," Phys. Rev. Accel. Beams **20**(4), 041302 (2017).
6. E. Curry, S. Fabbri, J. Maxson, P. Musumeci, and A. Gover, "Terahertz-based retrieval of the spectral phase and amplitude of ultrashort laser pulses," Phys. Rev. Lett. **120**(9), 094801 (2018).
7. D. Zhang, A. Fallahi, M. Hemmer, X. Wu, M. Fakhari, Y. Hua, H. Cankaya, A.-L. Calendron, L. E. Zapata, N. H. Matlis, and F. X. Kärtner, "Segmented terahertz electron accelerator and manipulator (STEAM)," Nat. Photonics **12**(6), 336–342 (2018).
8. C. Kealhofer, W. Schneider, D. Ehberger, A. Ryabov, F. Krausz, and P. Baum, "All-optical control and metrology of electron pulses," Science **352**(6284), 429–433 (2016).
9. F. Lemery, K. Flöttmann, T. Vinatier, and R. W. Assman, "A transverse deflection structure with dielectric-lined waveguides in the sub-THz regime," in "proceedings of IPAC," (2017).
10. D. Ehberger, A. Ryabov, and P. Baum, "Tilted electron pulses," Phys. Rev. Lett. **121**(9), 094801 (2018).
11. D. Ehberger, C. Kealhofer, and P. Baum, "Electron energy analysis by phase-space shaping with THz field cycles," Struct. Dyn. **5**(4), 044303 (2018).
12. D. Zhang, A. Fallahi, M. Hemmer, H. Ye, M. Fakhari, Y. Hua, H. Cankaya, A.-L. Calendron, L. E. Zapata, N. H. Matlis, and F. X. Kärtner, "Femtosecond phase control in high-field terahertz-driven ultrafast electron sources," Optica **6**(7), 872–877 (2019).
13. K. L. Vodopyanov, "Optical generation of narrow-band terahertz packets in periodically-inverted electro-optic crystals: conversion efficiency and optimal laser pulse format," Opt. Express **14**(6), 2263–2276 (2006).
14. S. Carbajo, J. Schulte, X. Wu, K. Ravi, D. N. Schimpf, and F. X. Kärtner, "Efficient narrowband terahertz generation in cryogenically cooled periodically poled lithium niobate," Opt. Lett. **40**(24), 5762–5765 (2015).
15. K. Ravi, D. N. Schimpf, and F. X. Kärtner, "Pulse sequences for efficient multi-cycle terahertz generation in periodically poled lithium niobate," Opt. Express **24**(22), 25582–5276 (2016).
16. A. S. Weling, B. B. Hu, N. M. Froberg, and D. H. Auston, "Generation of tunable narrowband THz radiation from large aperture photoconducting antennas," Appl. Phys. Lett. **64**(2), 137–139 (1994).
17. Z. Chen, X. Zhou, C. A. Werley, and K. A. Nelson, "Generation of high power tunable multicycle teraherz pulses," Appl. Phys. Lett. **99**(7), 071102 (2011).
18. F. Ahr, S. W. Jolly, N. H. Matlis, S. Carbajo, T. Kroh, K. Ravi, D. N. Schimpf, J. Schulte, H. Ishizuki, T. Taira, A. R. Maier, and F. X. Kärtner, "Narrowband terahertz generation with chirped-and-delayed laser pulses in periodically poled lithium niobate," Opt. Lett. **42**(11), 2118–2121 (2017).
19. S. W. Jolly, N. H. Matlis, F. Ahr, V. Leroux, T. Eichner, A.-L. Calendron, H. Ishizuki, T. Taira, F. X. Kärtner, and A. R. Maier, "Spectral phase control of interfering chirped pulses for high-energy narrowband terahertz generation," Nat. Commun. **10**(1), 2591 (2019).
20. M. M. Fejer, G. A. Magel, D. H. Jundt, and R. L. Byer, "Quasi-phase-matched second harmonic generation: Tuning and tolerances," IEEE J. Quantum Electron. **28**(11), 2631–2654 (1992).
21. Z. Cao, X. Gao, W. Chen, H. Wang, W. Zhang, and Z. Gong, "Study of quasi-phase matching wavelength acceptance bandwidth for periodically poled $LiNbO_3$ crystal-based difference-frequency generation," Opt. Lasers Eng. **47**(5), 589–593 (2009).
22. J. D. McMullen, "Chirped-pulse compresion in strongly dispersive media," J. Opt. Soc. Am. **67**(11), 1575–1578 (1977).

Optics EXPRESS


23. M. Miyagi and S. Nishida, "Pulse spreading in a single-mode fiber due to third-order dispersion," Appl. Opt. **18**(5), 678–682 (1979).
24. A. S. Weling and D. H. Auston, "Novel sources and detectors for coherent tunable narrow-band terahertz radiation in free space," J. Opt. Soc. Am. B **13**(12), 2783–2791 (1996).
25. S. Kamada, S. Murata, and T. Aoki, "On the chirp of narrowband terahertz pulses generated by photomixing with nonlinearly chirped laser pulse pairs," Appl. Phys. Express **6**(3), 032701 (2013).
26. T. Yoshida, S. Kamada, and T. Aoki, "Elimination of the chirp of narrowband terahertz pulses generated by chirped pulse beating using a tandem grating pair laser pulse stretcher," Opt. Express **22**(19), 23679–23685 (2014).
27. P. Ungelenk, M. Höner, H. Huck, S. Khan, C. Mai, A. M. auf der Heide, C. Evain, C. Szwaj, and S. Bielawski, "Continuously tunable narrowband pulses in the THz gap from laser-modulated electron bunches in a storage ring," Phys. Rev. Accel. Beams **20**(2), 020706 (2017).
28. S. W. Jolly, "Spectral phase manipulation of optical pump pulses for mJ-level narrowband terahertz generation in PPLN," Ph.D. thesis, Universität Hamburg (2017).
29. A. Curcio, V. Dolci, S. Lupi, and M. Petrarca, "Terahertz-based retrieval of the spectral phase and amplitude of ultrashort laser pulses," Opt. Lett. **43**(4), 783–786 (2018).
30. P. Y. Han and X.-C. Zhang, "Coherent, broadband midinfrared terahertz beam sensors," Appl. Phys. Lett. **73**(21), 3049–3051 (1998).
31. G. Gallot and D. Grischkowsky, "Electro-optic detection of terahertz radiation," J. Opt. Soc. Am. B **16**(8), 1204–1212 (1999).
32. J. R. Danielson, A. D. Jameson, J. L. Tomaino, H. Hui, J. D. Wetzel, Y.-S. Lee, and K. L. Vodopyanov, "Intense narrow band terahertz generation via type-II difference-frequency generation in ZnTe using chirped optical pulses," J. Appl. Phys. **104**(3), 033111 (2008).
33. Y.-S. Lee, W. C. Hurlbut, K. L. Vodopyanov, M. M. Fejer, and V. G. Kozlov, "Generation of multicycle terahertz pulses via optical rectification in periodically inverted GaAs structures," Appl. Phys. Lett. **89**(18), 181104 (2006).
34. I. Tomita, H. Suzuki, H. Ito, H. Takenouchi, K. Ajito, R. Rungsawang, and Y. Ueno, "Terahertz-wave generation from quasi-phase-matched GaP for 1.55 $\mu$m pumping," Appl. Phys. Lett. **88**(7), 071118 (2006).
35. A. Sell, A. Leitenstorfer, and R. Huber, "Phase-locked generation and field-resolved detection of widely tunable terahertz pulses with amplitudes exceeding 100 MV/cm," Opt. Lett. **33**(23), 2767–2769 (2008).
36. A. Cartella, T. F. Nova, A. Oriana, G. Cerullo, M. Först, C. Manzoni, and A. Cavalleri, "Narrowband carrier-envelope phase stable mid-infrared pulses at wavelengths beyond 10 $\mu$m by chirped-pulse difference frequency generation," Opt. Lett. **42**(4), 663–666 (2017).
37. Y. Fu, E. J. Takahashi, and K. Midorikawa, "High-energy infrared femtosecond pulses generated by dual-chirped optical parametric amplification," Opt. Lett. **40**(21), 5082–5085 (2015).
38. Y. Yin, X. Ren, Y. Wang, F. Zhuang, J. Li, and Z. Chang, "Generation of high-energy narrowband 2.05 $\mu$m pulses for seeding a Ho:YLF laser," Photonics Res. **6**(1), 1–5 (2018).
39. C. Vicario, A. V. Ovchinnikov, O. V. Chefonov, and C. P. Hauri, "Multioctave spectrally tunable strong-field terahertz laser," arXiv 1608.05319 (2016).
40. B. Liu, H. Bromberger, A. Cartella, T. Gebert, M. Först, and A. Cavalleri, "Generation of narrowband, high-intensity, carrier-envelope phase-stable pulses tunable between 4 and 18 THz," Opt. Lett. **42**(1), 129–131 (2017).
41. X. Wu, C. Zhou, W. R. Huang, F. Ahr, and F. X. Kärtner, "Temperature dependent refractive index and absorption coefficient of congruent lithium niobate crystals in the terahertz range," Opt. Express **23**(23), 29729–29737 (2015).
42. M. Unferdorben, Z. Szaller, I. Hajdara, J. Hebling, and L. Pálfalvi, "Measurement of refractive index and absorption coefficient of congruent and stoichiometric lithium niobate in the terahertz range," J. Infrared, Millimeter, Terahertz Waves **36**(12), 1203–1209 (2015).
43. M. Cronin-Golomb, "Cascaded nonlinear difference-frequency generation of enhanced terahertz wave production," Opt. Lett. **29**(17), 2046 (2004).
44. M. Hemmer, G. Cirmi, K. Ravi, F. Reichert, F. Ahr, L. Zapata, O. D. Mücke, A.-L. Calendron, H. Çankaya, D. Schimpf, N. H. Matlis, and F. X. Kärtner, "Cascaded interactions mediated by terahertz radiation," Opt. Express **26**(10), 12536–12546 (2018).
45. G. Tóth, J. Fülöp, and J. Hebling, "Periodically intensity-modulated pulses by optical parametric amplification for multicycle tunable terahertz pulse generation," Opt. Express **25**(23), 28258–28272 (2017).
46. Y.-S. Lee, T. Meade, T. B. Norris, and A. Galvanauskas, "Tunable narrow-band terahertz generation from periodically poled lithium niobate," Appl. Phys. Lett. **78**(23), 3583–3585 (2001).
47. P. Krogen, H. Suchowski, H. Liang, N. Flemens, K.-H. Hong, F. X. Kärtner, and J. Moses, "Generation and multi-octave shaping of mid-infrared intense single-cycle pulses," Nat. Photonics **11**(4), 222–226 (2017).
48. K. Ravi and F. X. Kärtner, "Simultaneous generation and compression of broadband terahertz pulses in aperiodically poled crystals," Opt. Express **27**(5), 6580–6597 (2019).
49. N. Belabas, J.-P. Likforman, L. Canioni, B. Bousquet, and M. Joffre, "Coherent broadband pulse shaping in the mid-infrared," Opt. Lett. **26**(10), 743–745 (2001).
50. Y. Yamaguchi, R. Hida, T. Suzuki, F. Isa, K. Yoshikiyo, L. Fujii, H. Nemoto, and F. Kannari, "Shaping and amplification of wavelength-tunable mid-infrared femtosecond pulses generated by intra-pulse difference-frequency mixing with spectral focusing," J. Opt. Soc. Am. B **35**(12), C1–C7 (2018).

Optics EXPRESS


51. K. Ravi, M. Hemmer, G. Cirmi, F. Reichert, D. N. Schimpf, O. D. Mücke, and F. X. Kärtner, "Cascaded parametric amplification for highly efficient terahertz generation," Opt. Lett. **41**(16), 3806–3809 (2016).
52. G. Cirmi, M. Hemmer, K. Ravi, F. Reichert, L. E. Zapata, A.-L. Calendron, H. Cankaya, F. Ahr, O. D. Mücke, N. H. Matlis, and F. X. Kärtner, "Cascaded second-order processes for the efficient generation of narrowband terahertz radiation," J. Phys. B: At., Mol. Opt. Phys. **50**(4), 044002 (2017).
53. Q. Zhang, E. J. Takahashi, O. D. Mücke, P. Lu, and K. Midorikawa, "Dual-chirped optical parametric amplification for generating few hundred mJ infrared pulses," Opt. Express **19**(8), 7190–7212 (2011).
54. Y. Yin, J. Li, X. Ren, Y. Wang, A. Chew, and Z. Chang, "High-energy two-cycle pulses at 3.2 $\mu$m by a broadband-pumped dual-chirped optical parametric amplification," Opt. Express **24**(22), 24989–24998 (2016).
55. Y.-S. Lee, T. Meade, V. Perlin, H. Winful, T. B. Norris, and A. Galvanauskas, "Generation of narrow-band terahertz radiation via optical rectification of femtosecond pulses in periodically poled lithium niobate," Appl. Phys. Lett. **76**(18), 2505–2507 (2000).
56. C. Vicario, B. Monoszlai, and C. P. Hauri, "GV/m single-cycle terahertz fields from a laser-driven large-size partitioned organic crystal," Phys. Rev. Lett. **112**(21), 213901 (2014).
57. B.-H. Chen, T. Nagy, and P. Baum, "Efficient middle-infrared generation in $LiGaS_2$ by simultaneous spectral broadening and difference-frequency generation," Opt. Lett. **43**(8), 1742–1745 (2018).
58. S. Bielawski, C. Evain, T. Hara, M. Hosaka, M. Katoh, S. Kimura, A. Mochihashi, M. Shimada, C. Szwaj, T. Takahashi, and Y. Takashima, "Tunable narrowband terahertz emission from mastered laser–electron beam interaction," Nat. Phys. **4**(5), 390–393 (2008).
59. J. G. Neumann, R. B. Fiorito, P. G. O'Shea, H. Loos, B. Sheehy, Y. Shen, and Z. Wu, "Terahertz laser modulation of electron beams," J. Appl. Phys. **105**(5), 053304 (2009).
60. C. Evain, C. Szwaj, S. Bielawski, M. Hosaka, Y. Takashima, M. Shimada, S. Kimura, M. Katoh, A. Mochihashi, T. Takahashi, and T. Hara, "Laser-induced narrowband coherent synchrotron radiation: Efficiency versus frequency and laser power," Phys. Rev. Spec. Top.–Accel. Beams **13**(9), 090703 (2010).
61. Y. Shen, X. Yang, G. L. Carr, Y. Hidaka, J. B. Murphy, and X. Wang, "Tunable few-cycle and multicycle coherent terahertz radiation from relativistic electrons," Phys. Rev. Lett. **107**(20), 204801 (2011).
62. M. Hosaka, N. Yamamoto, Y. Takashima, C. Szwaj, M. L. Parquier, C. Evain, S. Bielawski, M. Adachi, H. Zen, T. Tanikawa, S. Kimura, M. Katoh, M. Shimada, and T. Takahashi, "Saturation of the laser-induced narrowband coherent synchrotron radiation process: Experimental observation at a storage ring," Phys. Rev. Spec. Top.–Accel. Beams **16**(2), 020701 (2013).
63. A. Nguyen, P. G. de Alaiza Martinez, I. Thiele, S. Skupin, and L. Bergé, "THz field engineering in two-color femtosecond filaments using chirped and delayed laser pulses," New J. Phys. **20**(3), 033026 (2018).